

ÅBO AKADEMI UNIVERSITY
FACULTY OF SCIENCE AND ENGINEERING

Hydrogen reduction of iron oxides

Experimental study

Master's thesis

Nathalie Lillkaas

Åbo Akademi 2022

Carried out at the Process and Systems
Engineering Laboratory of Åbo Akademi
University under the supervision of prof.
Henrik Saxén and prof. Henrik Grénman.

ABSTRACT

Steel is one of the modern world's core pillars in engineering and construction materials, but the steel production causes large carbon dioxide emissions. The steel industry needs to reduce its carbon emissions to prevent global warming to exceed 2 °C. Today's ironmaking mainly uses carbon monoxide to reduce the oxygen from iron ore. The product from the use of carbon monoxide in iron oxide reduction is carbon dioxide. Replacing carbon monoxide with hydrogen would fundamentally reduce the greenhouse gas emissions. Hydrogen has been an interesting gas in iron oxide reduction for some time and the reaction kinetics have some advantages over reduction by carbon monoxide. The gaseous product from iron ore reduction with hydrogen is water vapor.

The analysis of the reduction is often based on equilibrium considerations, since the termination of the reduction is expected to be achieved at a specified temperature in equilibrium state. From a thermodynamic point a higher temperature is better for the hydrogen reduction reactions. A high temperature is also beneficial in terms of the kinetics.

In this thesis, experimental studies of iron oxide reduction with hydrogen have been undertaken to obtain data for mathematical modeling of the reduction reactions. The experiments have been done at Åbo Akademi University. To obtain information for an evaluation for the modeling work, isothermal experiments with powder samples of both hematite and magnetite were undertaken at different temperatures and at different gas flow rates. Experiments without any sample were also done to achieve a better calibration of the data. The sample size was 100 to 200 mg and the temperature in the experiments was between 400 °C and 900 °C, while the flow of hydrogen was between 4 ml/min and 20 ml/min. Argon was used as an inert gas in the experiments.

It appears from the results of the experiments that the temperature is the main parameter that affects the reduction time, and that the concentration of hydrogen in the mass flow has a significant impact on the results. Previous studies have shown similar results as the ones found in this thesis. However, some odd results were

obtained for gas of higher hydrogen concentration, and these were expected to be due to disturbances caused by water in the gas analyzed by a Mass Spectrometer. These problems should be solved in future work.

The aim of the experiments was to obtain data that could act as a starting point for a kinetic modeling of hydrogen reduction of hematite and magnetite. Despite the problems noted above, the experiments were reproducible and mostly successful, and the results have shed light on the reduction of iron oxide in hydrogen-containing gas mixtures.

TABLE OF CONTENTS

Abstract	2
Table of contents	4
Notations	6
1. Introduction	1
2. Background	3
2.1. <i>Ironmaking</i>	3
2.2. <i>Blast furnace</i>	3
2.3. <i>Direct Reduced Iron – DRI</i>	5
3. Theory	6
3.1. <i>Iron oxide reduction</i>	6
3.2. <i>Rate limiting steps</i>	8
3.3. <i>Reaction kinetics</i>	9
3.3.1. <i>Temperature</i>	9
3.3.2. <i>Pressure</i>	10
3.3.3. <i>Pellet/particle size</i>	10
3.4. <i>Earlier experiments</i>	12
4. Materials and methods	14
4.1. <i>Materials</i>	14
4.2. <i>Experiment</i>	14
4.2.1. <i>Equipment</i>	15
4.2.2. <i>Experiment setup</i>	16
5. Results and discussion	19
5.1. <i>Material analysis</i>	19
5.1.1. <i>Hematite</i>	19
5.1.2. <i>Magnetite</i>	20
5.2. <i>Results of the reduction experiments</i>	20
5.2.1. <i>Hematite vs. magnetite reduction</i>	21
5.2.2. <i>Hematite reduction under different temperatures</i>	23
5.2.3. <i>Hematite reduction for different hydrogen concentrations</i>	25
5.2.4. <i>Effect of sample size</i>	26
5.3. <i>Discussion</i>	27
5.4. <i>Conclusions and further studies</i>	31
6. Summary in Swedish – Svensk sammanfattning	33
7. References	37

Appendix 1	40
Appendix 2	43
Appendix 3	44

NOTATIONS

BET	– Brunauer-Emmett-Teller
DFT	– Density Functional Theory
DRI	– Direct Reduced Iron
GOD	– Gas Oxidation Degree
MS	– Mass Spectrometer
TCD	– Thermal Conductivity Detector

1. INTRODUCTION

About 5% of the earth's crust contains iron. It is, however, present mainly as iron oxides. Using reducing agent, metallic iron, Fe, can be extracted from the oxides. Iron is the main component in steel, which is used for a wide range of purposes: cars, ships, pipelines for gas and oil, electrical and mechanical machines, buildings, factories and so on. Therefore, the iron and steel industry is of great importance in the world and it provides material for the main structural engineering today. This industry sector is also of high economic importance; in 2020 about 1.8 billion tons crude steel was produced in the world.

The climate change that can be observed today is mainly due to increasing carbon dioxide, CO₂, emissions to the air. The iron and steel industry accounts for a large environmental impact. The direct CO₂ emissions from the iron and steel industry represents 7–9% of the total global emissions. (Spreitzer & Schenk, 2019)

The steel industry has an important role to play in standards of living worldwide and is absolutely necessary for modern life, but at the same time its emissions are damaging the environment. Due to its importance, the steel industry cannot be shut down to reduce CO₂ emissions. Instead, more environmentally friendly ways of steelmaking should be developed. (Ghosh & Chatterjee, 2008)

One way to reduce CO₂ emissions is to recycle the steel by re-melting it, because the primary process of extracting iron from iron ore is the main polluting process. (Ghosh & Chatterjee, 2008) As the need for steel is greater than the potential recycling quantities more steel must be extracted from the iron ore. To achieve an economic extraction of iron, rich deposits of iron ore are used. These are mainly iron ore with a Fe content above 55–60%, such as the iron oxide minerals hematite (Fe₂O₃) and magnetite (Fe₃O₄). (Ghosh & Chatterjee, 2008)

To reduce the CO₂ emissions in the iron and steel industry and achieve a more sustainable iron production a new way of reducing iron oxides is needed. In the last few years, researchers have actively investigated hydrogen, H₂, as an alternative to

carbon monoxide, CO, as the reducing gas. Hydrogen has a high calorific value, good thermal conductivity and a high reaction rate, because the molecule is small and has a high diffusion rate. All these characteristics of hydrogen give it great potential to be used as a reductant in the iron and steel making. (Liu, et al., 2020)

The development in the area of direct reduction has progressed over the years and in this thesis experiments with H₂ as reducing agent, instead of CO, have been performed in a laboratory environment. The results have been compared to findings of previous studies on the subject.

The experiments have been done at Åbo Akademi University at different temperatures and different mass flow rates of hydrogen and argon, Ar. The experiments have been performed to be able to study the reduction kinetics of iron ore powder and from that obtain kinetic parameters for mathematical modelling of ironmaking processes.

2. BACKGROUND

Steel is one of the modern world's core pillars in engineering and construction materials, and its demand is continuously increasing because of its large area of use and growing world population. (Wei, et al., 2018) However, the steel production causes large CO₂ emissions. Therefore, the steel industry needs to reduce its carbon emissions to prevent the global warming from exceeding 2 °C. (Hoffman, et al., 2020)

2.1. Ironmaking

The first ironmaking processes were driven by manpower and, therefore, the plants were small. Once the process to produce weapons of iron was learnt in the Iron Age, the ironmaking process was developed considerably. Over the years, the development of engineering and the ironmaking process has made it possible to increase the plant size and, thus, produce larger amounts of iron. (Ghosh & Chatterjee, 2008)

The foundation of today's ironmaking process is an old process that made its first appearance in the 15th century, much because of the realization that cast iron could be used to forge gun barrels. To produce iron, oxygen is removed by reduction of iron oxide. (Walker, 2017) The prehistoric furnaces were small, with a height of 1–1.5 m and a diameter varying from 0.4 to 0.8 m. (Ghosh & Chatterjee, 2008)

Iron ore is the raw material for the iron and steel industry. To release the iron from its chemical bond with oxygen and to melt the product are the primary objectives of iron making. Most of the iron production is done in blast furnaces while a smaller part of the production comes from so called direct reduction units. (Walker, 2017)

2.2. Blast furnace

Charcoal was the main fuel for the blast furnaces until the 18th century when coke as fuel was discovered. Coke is still being used and is more efficient than charcoal. Coke can support much larger furnaces than charcoal, but the fuel is hazardous for the environment and causes large amount of fossil CO₂ emissions. (Walker, 2017)

Over the years, the blast furnace has evolved, and improvements have been made to the process, resulting in an increase in iron production. However, the development of the process for converting the iron from blast furnace into wrought iron was not as fast. Instead, methods that allowed the furnace to operate at much higher temperatures, high enough to melt iron, were invented. This made producing steel possible. The operating principle of the blast furnace today is nearly the same as in the 18th century, but the size of a modern furnace has increased greatly. (Walker, 2017) The size of modern blast furnaces ranges from 20 to 40 meters high and diameters between 6 and 15 meters. (Gregersen, 2022)

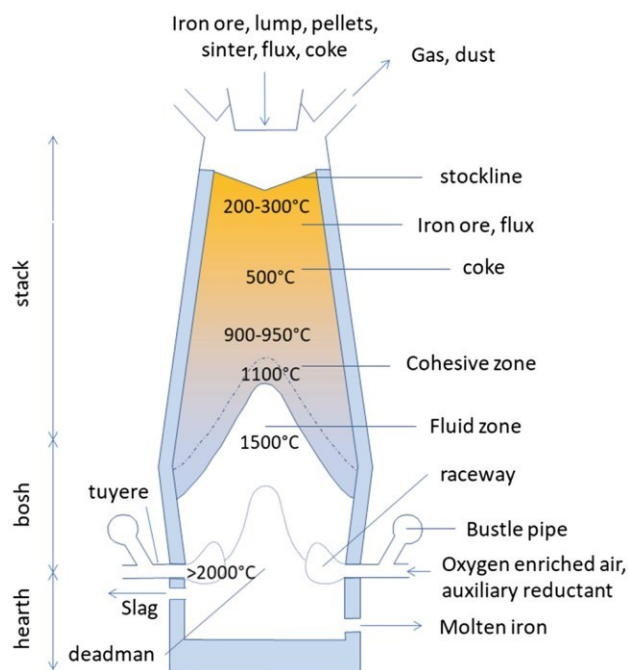


Figure 1 Blast furnace (Cavaliere, 2019)

Iron ore is charged at the top (Figure 1). As it descends, its temperature increases due to heat transfer from the ascending gas, which is formed by injecting preheated air through nozzles lower down in the furnace. When the temperature increases, the burden expands and, therefore, the furnace diameter is increased to allow the charge to move freely. Further down the melting of iron takes place. The molten iron dribbles to the furnace bottom and is tapped through a taphole in the lower sidewall of the furnace. By-products, such as slag and gas, are formed as well. Slag is also removed via the taphole while the gas exits the furnace at the top. (Walker, 2017) The blast furnace basic oxygen converter process is a large CO₂ emitter that accounted for 73.7% of the total production emissions. (Spreitzer & Schenk, 2019)

2.3. Direct Reduced Iron – DRI

New ironmaking processes were proposed throughout the 20th century, but a potential substitute for the blast furnace was not developed until 1950, when the direct reduction process of iron appeared. In this process a temperature below the metal's melting point is used to reduce iron ores. (Walker, 2017) To reduce the iron ore in the form of lumps, fines or pellets oxygen is removed using H₂ and CO. The main source of CO is natural gas and, therefore, the direct reduced iron is mainly produced where natural gas is available at low cost. This process decreases the need for coal and coke, which reduces the related emissions. (Yang, et al., 2013)

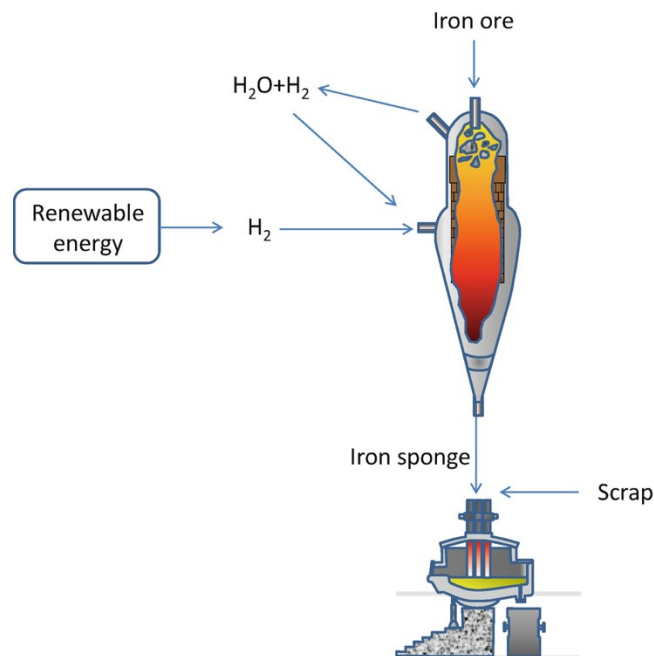


Figure 2 Direct reduction (Cavaliere, 2019)

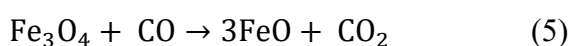
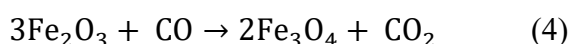
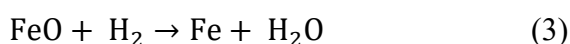
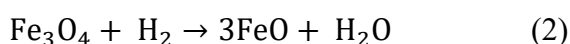
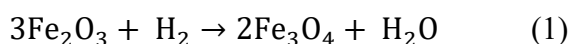
The most common processes for DRI in large-scale production are Midrex and HyL/Energiron. These are based on natural gas in shaft furnaces. In the DRI process, iron ore is charged at the top and a mixture of natural gas and H₂ is injected as fuel for the reduction process in the lower part of the shaft, as can be seen in Figure 2. Iron oxides react with the ascending gas and the heating is stopped at temperatures below the melting point for iron. The solid product, called DRI or sponge iron, is discharged from the bottom of the shaft after cooling to about 50 °C.

3. THEORY

The reduction of iron oxides occurs stepwise, with multiple factors that affect the rate of the reduction and the results. Previous experiments have observed the impact of different parameters on the reduction.

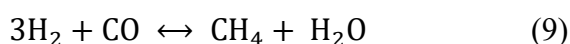
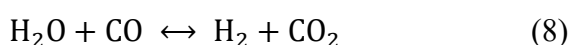
3.1. Iron oxide reduction

To reduce oxygen from the iron oxide, ores or pellets, reducing agents are needed. CO and H₂ are used as primary reducing agents according to the following heterogeneous chemical reactions:



Depending on the reducing gas, H₂ or CO, either water, H₂O, or CO₂ is formed when the iron oxides react. When hematite, Fe₂O₃, reacts with the reducing gas, it produces magnetite, Fe₃O₄. Further reaction of magnetite results in wüstite, FeO. Finally, wüstite reacts to produce metallic iron, Fe. It should be noted that the formulas above are simplified for the wüstite's part, as this is a species that takes a non-stoichiometric form, often expressed as Fe_xO, with x ≈ 0.95.

There are also some homogenous reactions that may occur among the different species in the reducing gas mixture. The following reactions are the most important of these (Ghadi, et al., 2020):



Carbon monoxide can form carbon and carbon dioxide (7). Carbon monoxide can also react with water to form hydrogen and carbon dioxide (8); this is called the water-gas shift reaction. Another possible reaction is that hydrogen reacts with carbon monoxide forming methane, CH₄, and water (9). The reverse is the primary reaction in reformation of natural gas.

At temperatures above 843 K the hydrogen-based reduction proceeds from hematite via magnetite to wüstite and finally to iron. At temperatures below 843 K, a reduction directly from magnetite to metallic iron occurs, as can be seen in the Baur-Glässner diagram in Figure 3. (Spreitzer & Schenk, 2019)

The reduction of pure hematite thus follows the steps $\text{Fe}_2\text{O}_3 \rightarrow \text{Fe}_3\text{O}_4 \rightarrow \text{FeO} \rightarrow \text{Fe}$, with the corresponding reduction degrees of $0\% \rightarrow 11\% \rightarrow 33\% \rightarrow 100\%$, which express the ratio of the removed oxygen and the initial oxygen in hematite.

To achieve the highest utilization of the reducing gas, the termination of the reduction is expected to be at a specified temperature in the equilibrium state. Therefore, the reduction analysis is often based on the equilibrium diagram. (Chen, et al., 2019)

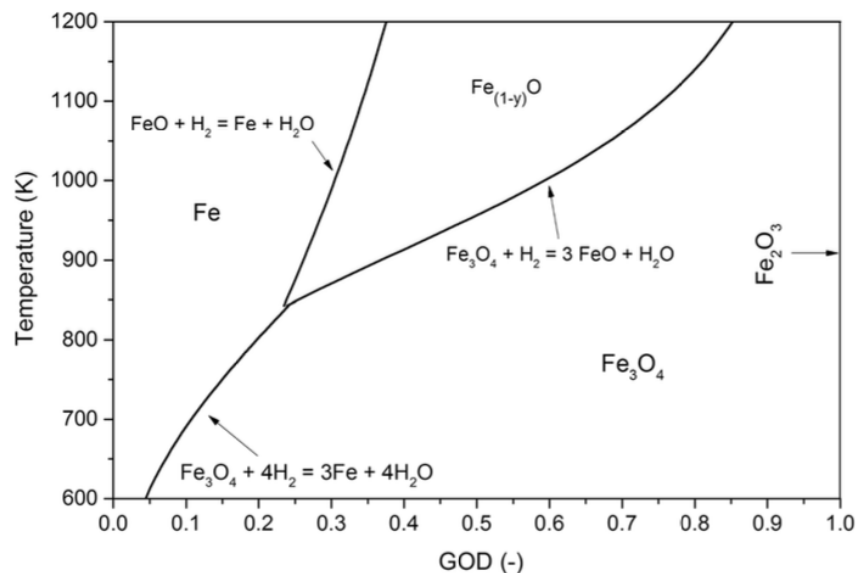


Figure 3 Baur-Glässner diagram for Fe-O-H₂ system (Spreitzer & Schenk, 2019)

Figure 3 shows the Baur-Glössner diagram for the Fe-O-H₂ system with respect to temperature and Gas Oxidation Degree (GOD). The stability areas for different iron oxide phases are shown depending on the temperature and GOD. The definition for GOD is the ratio of oxidized gas components over the sum of the oxidized and oxidizable compounds. (Spreitzer & Schenk, 2019)

In the diagram it can be seen that any concentration of H₂ (i.e., GOD < 1) can reduce hematite to magnetite, and that an increasing temperature results in an expanding stability area for metallic iron and wüstite. Wüstite is seen to be in a stable phase only above a certain temperature (about 845 K). A lower GOD characterizes a higher reduction force for the gas mixture. This indicates that, from a thermodynamic point of view, the reduction with H₂ should be carried out at the highest possible temperature. (Spreitzer & Schenk, 2019) With lower temperatures the stability area for Fe is smaller and, thus, the conditions have to be more reducing to produce Fe.

3.2. Rate limiting steps

The rate of a chemical reaction is dependent on the slowest step of the reaction, called the rate limiting step. Both thermodynamics and kinetics affect the process productivity and affect the total efficiency of the reduction process. (Spreitzer & Schenk, 2019)

Experimental observations from reducibility tests that have been conducted indicate that the factor that is most important in controlling reducibility is the porosity of the iron ore particle. (Ghadi, et al., 2020) Studies show that with increasing reduction temperature the porosity increases and, thus, the increasing temperature results in an effective diffusivity increase. (Ghadi, et al., 2020) The reduction rate was experimentally shown to be significantly slower at lower temperature and pressure.

A higher temperature increases the reduction rate also in terms of kinetics because of the limiting effects regarding diffusion and nucleation. The Arrhenius equation (10) is a mathematical expression which describes the effect of the temperature on the rate of the chemical reactions. According to the equation, an increasing

temperature will lead to a reduction rate that is exponentially increasing (Spreitzer & Schenk, 2019)

$$k = Ae^{-\frac{E_a}{RT}} \quad (10)$$

where k is the reaction rate constant, A is the frequency at which the molecules and atoms collide, $R = 8.314 \text{ J}/(\text{mol}\cdot\text{K})$ is the ideal gas constant, E_a is the activation energy and T is the thermodynamic temperature. (Gregersen, 2019)

Previous studies done by El-Gleassy et al. (1994) conclude that the reduction rate gradually increased with temperature. It was also shown from calculations of the activation energy that gas diffusion is the rate limiting step at the initial stage of reduction, whereas both gas diffusion and interfacial chemical reaction were the rate limiting steps in the later stage. In their experiment, the authors used iron ore powder with pure hydrogen as reducing gas at 973 K to 1273 K. (El-Gleassy, et al., 1994)

3.3. Reaction kinetics

For reduction with H_2 the reaction is endothermic, meaning that to guarantee a constant reduction temperature, energy must be supplied to the system. Temperature, gas composition and pressure are factors that affect the reduction rate. Besides these, pellet size, morphology and porosity profoundly affect the reduction rate. The following subsections briefly discuss the influence of different factors and report some earlier experimental work in the field.

3.3.1. Temperature

The temperature is, as seen above in the Arrhenius equation (10), a factor that theoretically strongly affects the reduction rate and, therefore, influences how fast the iron oxides can be reduced. Experiments done by El-Geassy and Nasr (1988) showed that increasing temperature resulted in increasing reduction rate. The temperature also affects the structure of the DRI. With a decrease in temperature, the pore structure becomes finer, while an increase in reduction temperature results in a decrease in the total pore area. (El-Geassy & Nasr, 1988)

Figure 4 shows the observed reduction degree (RD) of pellets in experiments performed at different temperatures. As can be seen, higher temperatures result in a noticeably faster reduction rate. (Spreitzer & Schenk, 2019)

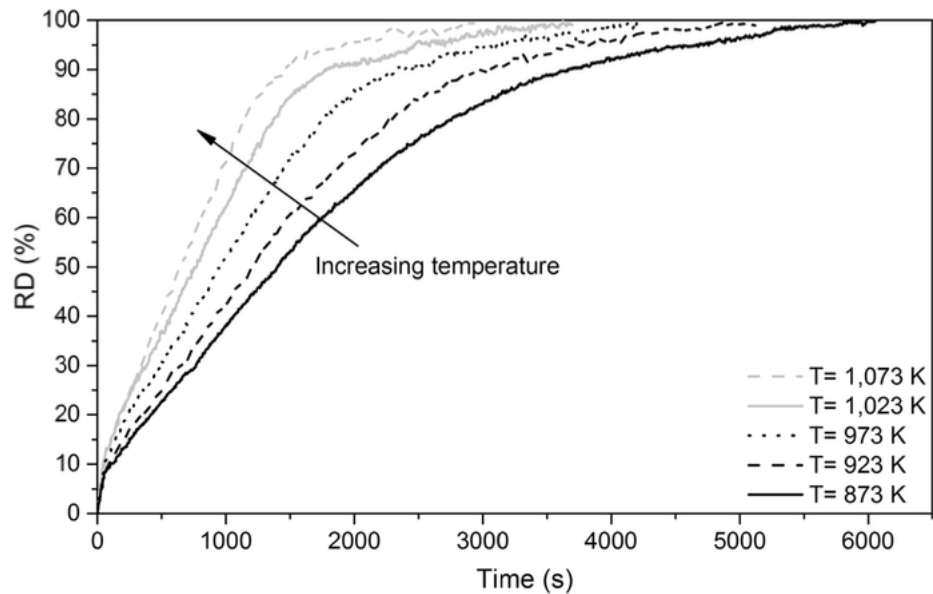


Figure 4 Comparison of the progress of reduction at different temperatures (Spreitzer & Schenk, 2019)

3.3.2. Pressure

The impact on the reduction rate of the absolute pressure and partial pressure of H_2 has also been studied. In one study (Habermann, et al., 2000) examined the difference in reduction rate with atmospheric and elevated pressures. The tests demonstrated that increasing the absolute pressure, and keeping the partial pressure of H_2 constant, did not lead to any notable change in the reduction rate in the early and medium stages. As expected, an increase in the partial pressure of H_2 , however, led to a higher reduction rate. A higher partial pressure of H_2 corresponds to a higher concentration of H_2 which, according to the authors, could explain the higher reduction rate. (Habermann, et al., 2000)

3.3.3. Pellet/particle size

The relation between the reduction time and the iron oxide pellet size has been studied in multiple investigations. Table 1 shows the time it took for the reduction to reach completion for various reactions with different pellet sizes and temperatures.

Table 1 Reduction time depending on pellet size

Pellet diameter [mm]	Gas	Mass flow H ₂ [l/min]	Temperature [K]	Time [min]	Source
12	Pure H ₂	5	1273	19.5	(Zuo, et al., 2015)
12	Pure H ₂	5	1173	25.8	(Zuo, et al., 2015)
12	Pure H ₂	5	1073	37.5	(Zuo, et al., 2015)
11.25 (type 1)	Pure H ₂	2	1073	22.5	(Kazemi, 2016)
11.25 (type 1)	Pure H ₂	2	1123	17.5	(Kazemi, 2016)
11.25 (type 2)	Pure H ₂	2	1073	22	(Kazemi, 2016)
11.25 (type 2)	Pure H ₂	2	1123	12.5	(Kazemi, 2016)
10.7	Pure H ₂	2	1123	15	(Bonalde, et al., 2005)
10.7	H ₂ , CO	2	1123	30	(Bonalde, et al., 2005)

The impact of the size of the iron oxide pellets depends on the porosity. The impact of the size is smaller if the pellets are very porous, and bigger if they are less porous. For a more porous particle, the reducing gas is able to penetrate the particle and, thus, the reduction can start at the same time at all surfaces. Also, a porous particle has less reactants (on a volume basis).

For iron oxide particles it can be recognized that the reduction rate is decreasing with increasing sizes of the particles. The fractional reduction was however the same at the completion of the reduction. (Habermann, et al., 2000)

For particles larger than 500 μm using CO/CO₂ gas mixtures, the reduction rate is decreasing according to Corbari & Fruehan (2010). At lower temperatures the size of the particles has less impact on the reduction rate as other rate-limiting steps are central in these cases. (Spreitzer & Schenk, 2019)

3.4. Earlier experiments

Pineau et al. (2005) studied the reduction of hematite by H₂ in a temperature range between 220 °C and 680 °C, with the goal to examine the rate-controlling process. According to the literature the authors quoted, the activation energy, E_a , is dependent on the raw material composition and structure, temperature range, nature of reducing gas, reaction step, presence of water vapor, impurities and so on. In their literature study, the authors found that the reported activation energy varies enormously, from 18 kJ/mol to 246 kJ/mol. Based on the experiments it was concluded that the activation energy for reduction from hematite to magnetite was 76 kJ/mol, from magnetite to metallic iron 88 kJ/mol, at temperatures lower than 417 °C and 39 kJ/mol at temperatures higher than 417 °C. (Pineau, et al., 2005)

Experiments done by Kazemi show that the reduction rate was higher at 1123 K compared to at 1073 K. In the experiments, three different types of iron oxide pellets, two types of commercial samples and one pure hematite sample with high density, were isothermally reduced by H₂. It was recognized that the dense sample diffusion played a more significant role in controlling the rate than for the more porous commercial pellet. (Kazemi, 2016)

Fruehan et al. (2005) did experiments on the final stage of iron ore reduction by H₂. In the experiments, hematite particles with a size of 180-250 μm , and flow rates 0.5–3 L/min of hydrogen, were tested. From the experiments, it was noted that at flow rates above 2 L/min the reduction rate did not change, which indicated that the external mass transfer resistance could be neglected in this region. These results showed that the reduction rate was significantly slower at lower temperature and pressure. (Fruehan, et al., 2005)

Elzohiery et al. (2016) reported iron oxide reduction experiments with H₂ as reducing gas, at temperatures varying from 1150 °C to 1350 °C, using magnetite concentrate particles with different size fractions. The magnetite concentrate particles were 20–25 μm, 32–38 μm and 45–53 μm in diameter. From the experiments, the authors concluded that the particle size had a relatively small effect on the reduction rate within the studied size ranges. They found that an activation energy of 193 kJ/mol characterized the experimental results. (Elzohiery, et al., 2016)

In summary, it can be concluded that the range of activation energies reported for iron oxide reduction by H₂ are large and that obviously the properties of the raw material plays an important role for the rate of the reduction reactions.

4. MATERIALS AND METHODS

In the present work, reduction experiments were undertaken in an AutoChem 2910 analyzer, produced by Micromeritics. Hematite and magnetite were used as samples, and some experiments were run without samples for comparison. The main setup was the same in all experiments, which were performed isothermally at atmospheric pressure.

4.1. Materials

In the experiments, hematite and magnetite from Sigma-Aldrich were used. The hematite in the experiment had an average particle size $< 5 \mu\text{m}$ and a purity of 96%. The magnetite had an average particle size $< 5 \mu\text{m}$ and a purity of 95%. Figure 5 shows samples of hematite and magnetite powder used in the experiments. Surface area analyzes have been done for both hematite and magnetite powder.

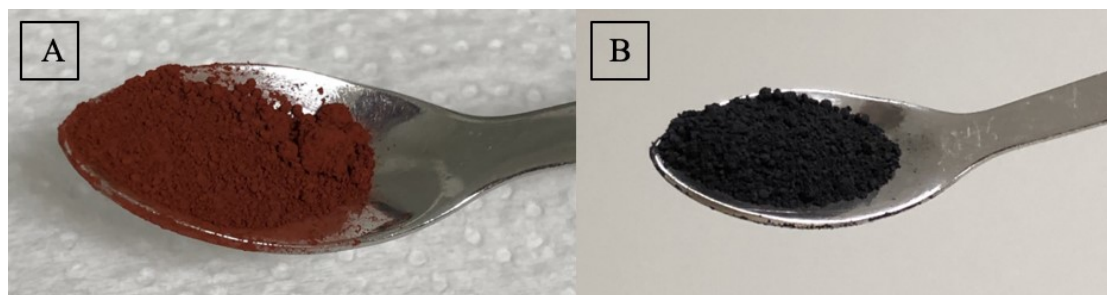


Figure 5 Hematite powder (A), magnetite powder (B)

4.2. Experiment

To be able to evaluate the reduction of hematite and magnetite by H_2 , various reduction experiments have been undertaken. The experiments were performed at different temperatures, and with different gas flow rates. Some experiments were done without a sample to get a baseline for the analysis, Table 2. In the experiments, argon, Ar, was used as inert gas.

4.2.1. Equipment

Micromeritics AutoChem 2910 is an automated catalyst characterization system that was used to conduct the reduction experiments in the present work. The system has Windows software to control the process. The software monitors the progress in every step of the experiment and controls the temperature and gas flows. Sample information and conditions for the experiments are specified by the operator. The furnace temperature, from -120 to 1100 °C, the duration and the ramp-up time can be set. The flow rates of the gases are controlled by the mass flow controllers and are set in the sample's analysis file.

The Thermal Conductivity Detector (TCD) has high accurate gold-plated filaments that detect changes in the thermal conductivity of the gases. To detect the thermal conductivity, it measures the difference between the gas that flows over the sample and the reference filaments. The thermal conductivity of the gas determines how quickly the gas removes heat from the detector. A high thermal conductivity cools the filaments quickly, thus, it requires more power to maintain the temperature.

The gas that reacts with the sample causes changes in the composition of the gas which consequently change the thermal conductivity. These changes are sensed by the detector and compared with the reference gas that has not passed the sample. The detector reports the voltage required to keep the temperature constant. AutoChem has an exhaust gas analysis port that allows the gas to be measured by a separate Mass Spectrometer (MS) after it has passed the TCD.

The Mass Spectrometer used in the experiments was a Balzer Instrument Gas analysis system GSD 300 O with Windows software that collects the results from the measurements. It is a quadrupole Mass Spectrometer, which means it has four charged cylindrical rods placed parallel to each other. It measures the ions from the sample based on the mass-to-charge ratio. A radiofrequency and direct current generator are connected to the rods. The ions are constrained to follow a path between the rods until they reach the detector where they are scanned. The MS is equipped with two different detectors, Faraday and Channeltron. The Channeltron detector was used in the experiments because of its higher sensitivity.

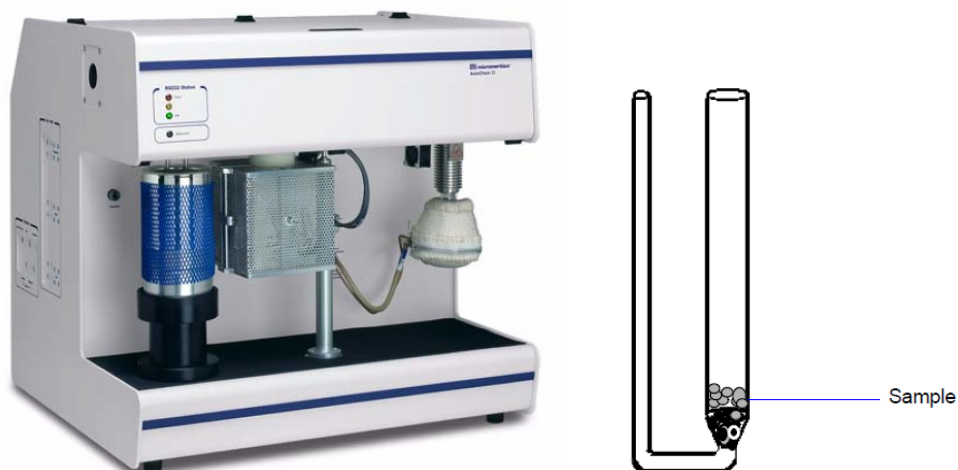


Figure 6 Picture of experiment equipment (left) drawing of the tube with quartz wool and sample (right)

4.2.2. Experiment setup

To prepare the experiments quartz wool was placed in the sample tube, see Figure 6, and the iron oxide powder was weighed to obtain a desired sample mass. The iron oxide powder was then placed on the quartz wool in the tube. When the sample was placed in the tube and the tube was put in position, the conditions for the experiment were stated in the computer program. The conditions were set to ramp up the temperature to the aim temperature for each experiment. The hold time at the aim temperature was also set. Argon and Hydrogen gases were obtained from compressed gas cylinders and the mass flows of the gases were controlled by the conditions set in the computer program.

At the beginning of each experiment argon gas was let through the system until it reached the desired temperature. The temperature ramp-up rate chosen was 10 °C/min (Figure 7). When the desired temperature was achieved, the valve to the hydrogen cylinder was manually opened. The argon atmosphere was kept constant during both heating and cooling.

After the gas had passed the reaction tube it went through the MS, where the different gas substances were measured. When the experiment was finished, the results from the MS were saved to the computer and the cooling of the system started. It should be noted that the gas enters the sample bed from above and leave the bed in the bottom to enter the pipe segment with smaller diameter, Figure 6.

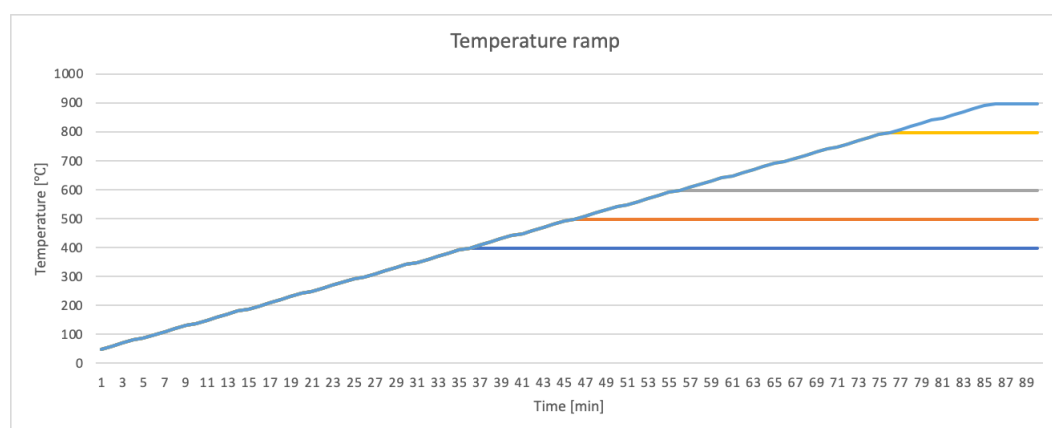


Figure 7 Temperature ramp-up for five different experiments

The experiments were, as seen in Table 2, carried out at temperatures between 400 °C and 900 °C. The mass flow of hydrogen varied from 2 ml/min to 20 ml/min and the mass flow of argon varied from 0 ml/min to 24 ml/min.

The measured data from the experiments were saved to the computer and extracted to an Excel file. The Excel file was imported to Matlab from where graphs were produced to show the results of the experiments.

Table 2 Experiments undertaken in the thesis

		Mass [mg]	Temperature [°C]	Flow rate H ₂ [ml/min]	Flow rate Ar [ml/min]
1	Hematite	96.5	400	2	18
2	Hematite	103.4	400	4	4
3	Hematite	100	400	4	16
4	Hematite	96.9	500	2	18
5	Hematite	97.0	500	4	4
6	Hematite	102.2	600	2	18
7	Hematite	110.0	600	4	4
8	Hematite	100	600	4	16
9	Hematite	145.6	800	4	4
10	Hematite	114	800	4	8
11	Hematite	208	800	4	8

12	Hematite	104	800	4	16
13	Hematite	200.1	800	4	16
14	Hematite	107.4	800	4	24
15	Hematite	102.9	900	4	24
16	Magnetite	114.6	600	20	0
17	Magnetite	100	600	4	16
18	Magnetite	104.7	800	4	16
19	Magnetite	203.4	800	4	16
20	Blank		500	4	16
21	Blank		600	4	16
22	Blank		800	4	16

5. RESULTS AND DISCUSSION

The main results of the analysis of the material and experiments are presented in this chapter. Due to the relatively large number of experiments, all results are not presented, but the data is made available for analysis later for other researchers at the laboratory. Results from the TCD and MS were saved to an Excel file and analyzed in Matlab 2021b, to obtain graphs that show how the reduction progresses during the experiments. The results from the experiments were also used for comparison with a mathematical model of a system developed by Salucci (2022).

5.1. Material analysis

To analyze the surface and texture properties of the hematite and magnetite used in the experiments, the Brunauer-Emmett-Teller (BET) and the Density Functional Theory (DFT) methods were used.

BET is applied to determine the specific area of porous materials. The specific area is determined by isothermal nitrogen absorption measurements. Multilayer adsorptions of gas are assumed on the adsorbent's surface. (Pourhakkak, et al., 2021) To determine the pore volume/pore size distribution DFT was used.

The instrument that was used was a Micromeritic 3 Flex 3500 and the mass of the samples tested was approximately 100–250 mg. The external pretreatment was done at 200 °C overnight and the internal pretreatment was done at 180 °C for 14h.

5.1.1. Hematite

The hematite analysis resulted in a surface area of $7.6308 \pm 0.0744 \text{ m}^2/\text{g}$ (Figure 8). For comparison it may be noted that El-Geassy and Nasr studied the physical characteristics of green hematite compacts and determined a surface area of $7.31 \text{ m}^2/\text{g}$ (El-Geassy & Nasr, 1988), which is in overall agreement with the present findings.

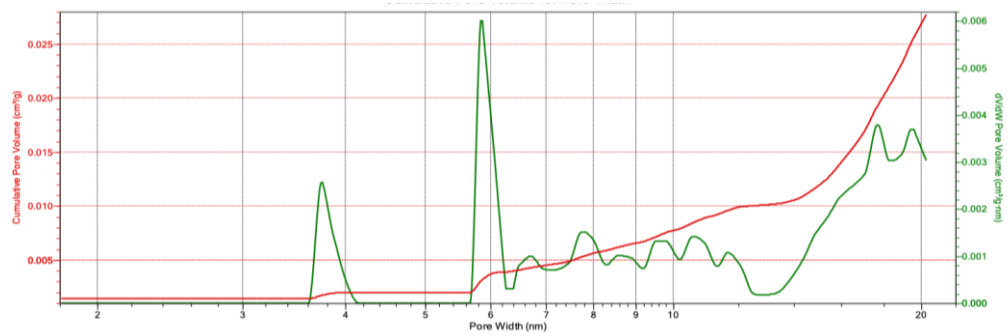


Figure 8 Cumulative pore volume vs. pore width for hematite, red line: cumulative pore volume, green line: pore volume

5.1.2. Magnetite

The magnetite analysis resulted in a clearly lower surface area of 3.7057 ± 0.0129 m²/g, see Figure 9. Figure 9 shows the cumulative pore volume vs. the pore width for the magnetite used in the experiments.

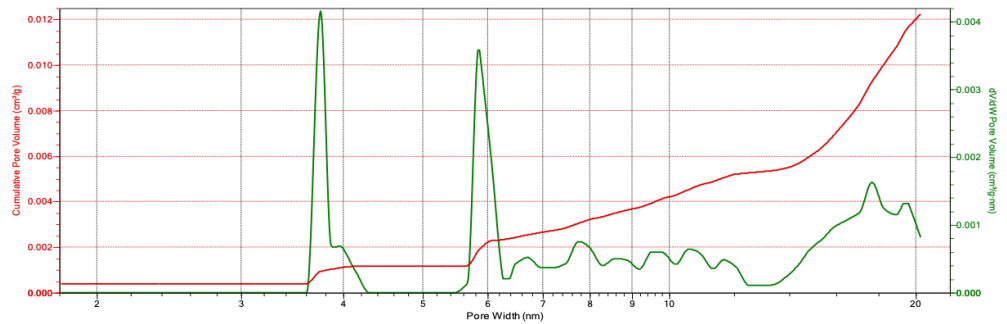


Figure 9 Cumulative pore volume vs. pore width for magnetite, red line: cumulative pore volume, green line: pore volume

5.2. Results of the reduction experiments

In the following, some results of the reduction experiments undertaken in the work are presented. Since the feed hydrogen flow rate was constant, 4 ml/min, in all experiments to be reported, the hydrogen signal from the MS of the outgoing gas was normalized to yield this value at full conversion of the sample, and the results of several experiments were plotted in the same figure. For the case of simplicity, the signal from the MS and the concentration were assumed to be proportional, since a separate calibration undertaken before the present work (Ghosh 2022) indicated quite linear relations. The specific experiments depicted are referred to by the experiment number reported in the first column of Table 2.

5.2.1. Hematite vs. magnetite reduction

The first reduction experiments undertaken in the work studied the reduction of 100 mg samples of hematite and magnetite at 600 °C, with a gas flow rate of 16 ml/min Ar and 4 ml/min H₂, to analyze the overall differences in the reduction behavior of the two oxides. Theoretically, magnetite has 11% less oxygen than hematite, but as the initial sample mass was (practically) identical, the oxygen content of the samples differed a bit more. For the sake of simplicity, assuming a mass of 100 mg and 95% purity for both samples, the molar amounts of hematite and magnetite are $0.095 \text{ g} / (159.7 \text{ g/mol}) = 0.595 \text{ mmol}$ and $0.095 \text{ g} / (231.6 \text{ g/mol}) = 0.410 \text{ mmol}$, where the denominators are the molar mass of hematite and magnetite, respectively. Thus, from the stoichiometry, the molar amounts of oxygen in the two samples are 1.785 mmol and 1.641 mmol. Since one mol of oxygen consumes one mole of H₂, the magnetite sample should require $(1.785-1.6141)/1.785 = 8\%$ less hydrogen to become fully reduced.

Figure 10 shows the outflow rates of hydrogen “normalized” to become identical with the target inflow rate (4 ml/min) when the curves level off and the reactions presumably have been completed. The results for the hematite and magnetite samples are depicted in red and blue, respectively. Since the moment when the experiment started was not recorded very accurately, the curves have been shifted in time to show the initial increase simultaneously. The two curves are practically identical for the first 50 minutes of the experiment, and the differences may fall within the accuracy of the measurement. However, for $t = 50\text{--}80 \text{ min}$, the hematite sample shows faster reduction, despite the larger oxygen content of the initial sample. This may be ascribed to a better reducibility of hematite than magnetite, which is a well-known phenomenon and can be explained by the structural changes in the particles that occur during the reduction of hematite to magnetite. (Weiss, 2010)

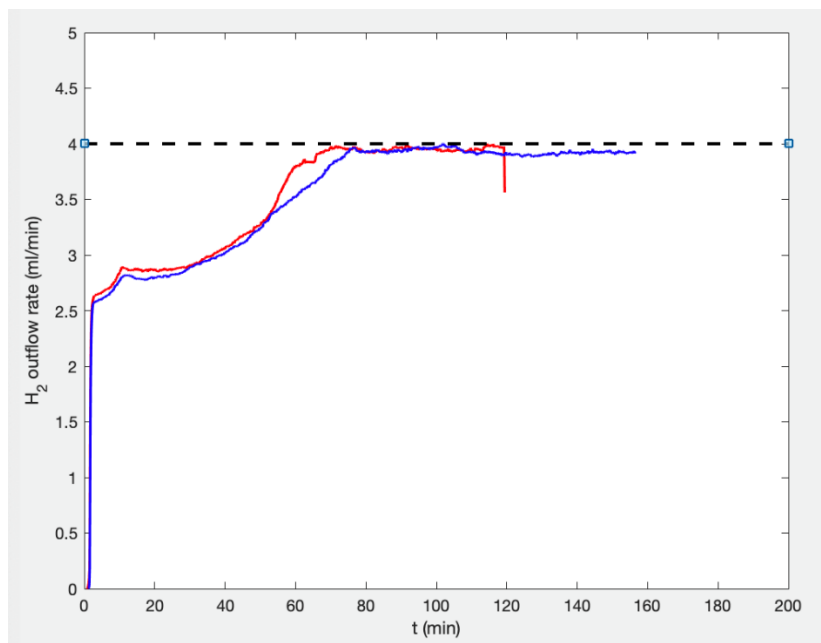


Figure 10 Hematite (experiment (8) in Table 2) vs magnetite (17) hematite red line, magnetite blue line

Despite the different appearances of the curves noted for the final stages of the reduction, the other characteristics can be qualitatively explained by the equilibrium diagram, which has been reproduced in Figure 11 with auxiliary lines at three different temperatures indicating the equilibrium conditions. At 600 °C, the oxidation degree of the gas must not exceed 31% to make it possible to reduce magnetite to wüstite, while the limit for reducing wüstite to metallic iron is 25%. Assuming proportionality between the MS signal and the hydrogen concentration, the two plateaus (the first of which is less obvious in the figure) observed at hydrogen outflow rates of about 2.5 ml/min and 2.8 ml/min correspond to oxidation degrees of $(4-2.5)/4 = 37\%$ and 32% of the outlet gas. Even though these values are about 5 percent points higher than the corresponding equilibrium values, the results seem to indicate that the hydrogen content of the gas decreases so much when passing through the upper part of the sample bed, that equilibrium is reached, and the lower parts cannot be reduced until the hydrogen consumption in the upper bed decreases (as the iron oxides in the upper layers become more fully reacted). The offset in the gas composition compared to the ones in the equilibrium diagram can possibly be explained by a nonlinear relation between the MS signal and the gas concentration.

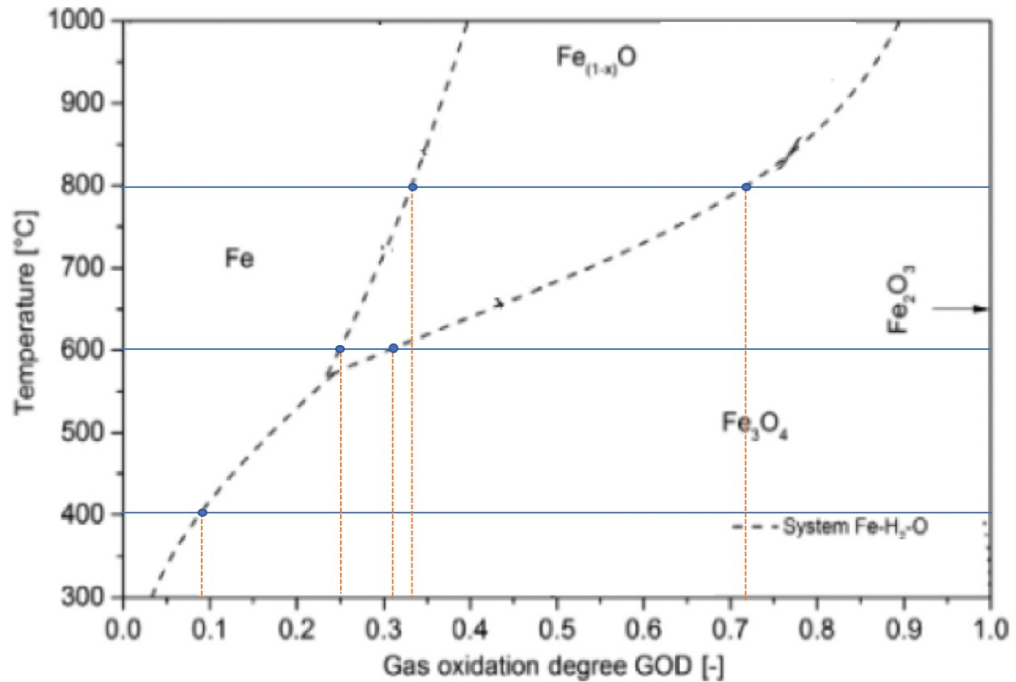


Figure 11 Equilibrium diagram

5.2.2. Hematite reduction under different temperatures

The next set of experiments study the effect of temperature on the reduction of hematite, undertaking the experiments at 400 °C, 600 °C and 800 °C. Figure 12 depicts the normalized outflow rates of H₂, illustrating the marked effect of temperature on the reduction rates. At the lowest temperature (400 °C, green line) the initial reduction is still fast but after a small plateau, the reduction progresses as a slow but rather constant speed and the sample was not fully reduced within 200 min of reaction (but continued for about 100 minutes).

As for the intermediate temperature (600 °C, blue line), the curve is shifted to lower hydrogen content showing two plateaus during the first 60 minutes, after which the reduction soon becomes completed and the curve levels off (at $t \approx 70$ min). For the highest temperature (800 °C, red line) the plateaus are shifted downward and a new plateau at a hydrogen outflow rate of about 3.4 ml/min is noted.

The equilibrium diagram in Figure 11 indicates that since wüstite is not in a stable phase at 400 °C, a single equilibrium (between magnetite and metallic iron) should occur at a gas oxidation degree of 9%. In Figure 12, this should be seen as a plateau

at an outflow rate of about 3.6 ml/min, not very different from the stable level seen for the green line. For the experiment at 600 °C the plateaus were already discussed in subsection 5.2.1. For the experiment at the highest temperature, 800 °C, the gas oxidation degrees at equilibrium are 72% and 33% (Figure 11). These correspond to outflow rates of hydrogen of 1.1 ml/min and 2.7 ml/min, not very different from the first two plateaus observed for the red curve in Figure 12. The third plateau at a hydrogen flow of 3.4 ml/min, as well as the one at the same level for the experiment undertaken at 400 °C, cannot be explained by equilibrium arguments. The likely reason for this was later concluded to be a disturbance of the MS signal caused by water in the gas flow. It is, furthermore, likely that the offsets observed from the expected equilibrium conditions of the other plateaus can be explained by the detrimental effect of water on the analysis.

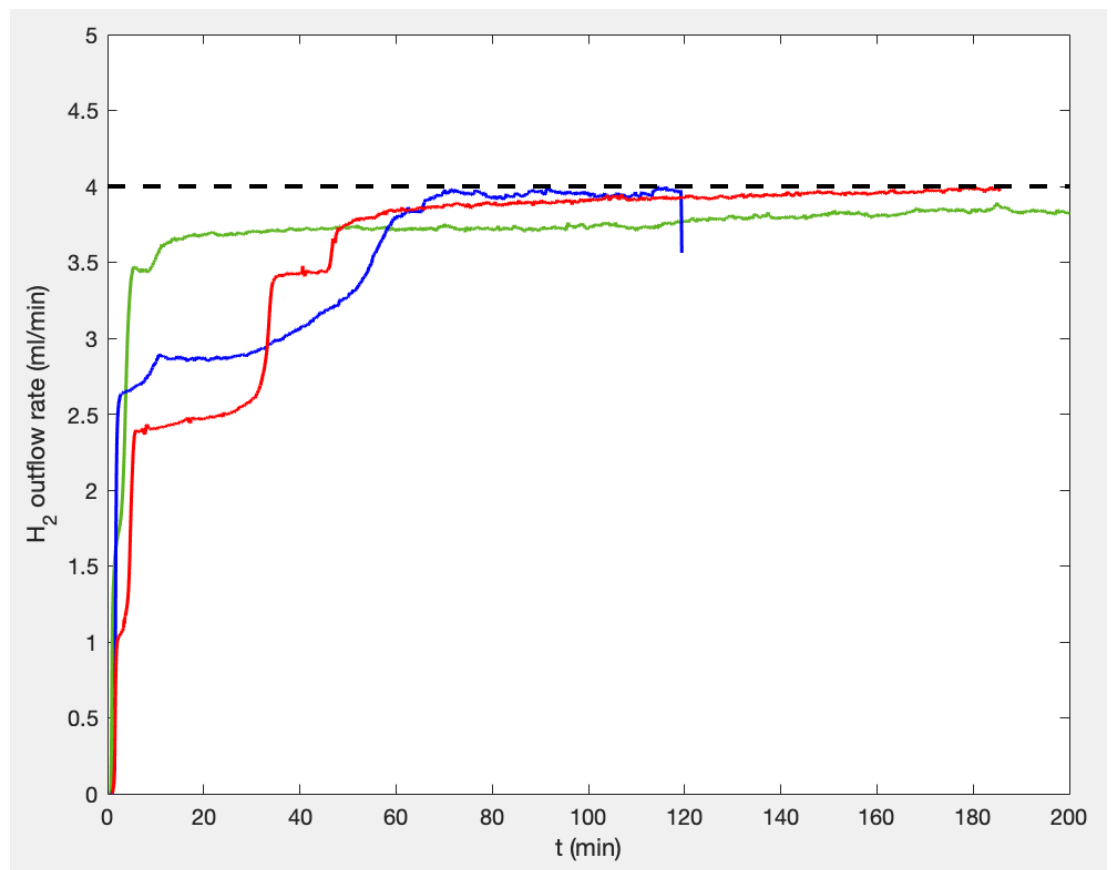


Figure 12 Hematite 400 °C green (3), 600 °C blue (8), 800 °C red (12)

5.2.3. Hematite reduction for different hydrogen concentrations

The role of the H₂ concentration was studied in this work mainly by adjusting the flow rate of the inert gas, Ar, keeping the flow rate of H₂ fixed at 4 ml/min.

The next set of experiments study the effect of H₂ concentration on the reduction of hematite at a temperature of 800 °C. Figure 13 depicts the H₂ outflow rates for the cases where the argon flow was 4 ml/min (Experiment 9, green line), 8 ml/min (experiment 10, purple line), 16 ml/min (experiment 12, blue line), and 24 ml/min (Experiment 14, red line). While the initial part of the results are very equal, the unexpected final plateau (at a H₂ outflow rate of about 3.5 ml/min) appears for all experiments except for the experiments at the lowest hydrogen concentration. This indicates water as the potential cause of the problems in the analysis. At increasing feed of hydrogen concentrations, the resulting water vapor concentration in the system naturally increases, giving rise to more pronounced problems.

Disregarding this flaw of the results, and focusing on the first part of the experiments, one may note that the first two plateaus (which should theoretically occur at outflow rates of 1.1 ml/min and 2.7 ml/min, see subsection 5.2.2) occur at very similar levels in the different experiments, as expected, since the equilibrium conditions should be the same at the constant temperature. It is still interesting to note that small differences in the level of the second plateau occurs hand by hand with the H₂ concentration of the feed flow. Disregarding the third plateau, it is also worth noting that the end of the final plateau, which most likely represents the time point where the reduction reactions come to completion, occurs later the higher the concentration of H₂ in the feed flow is, which is somewhat surprising.

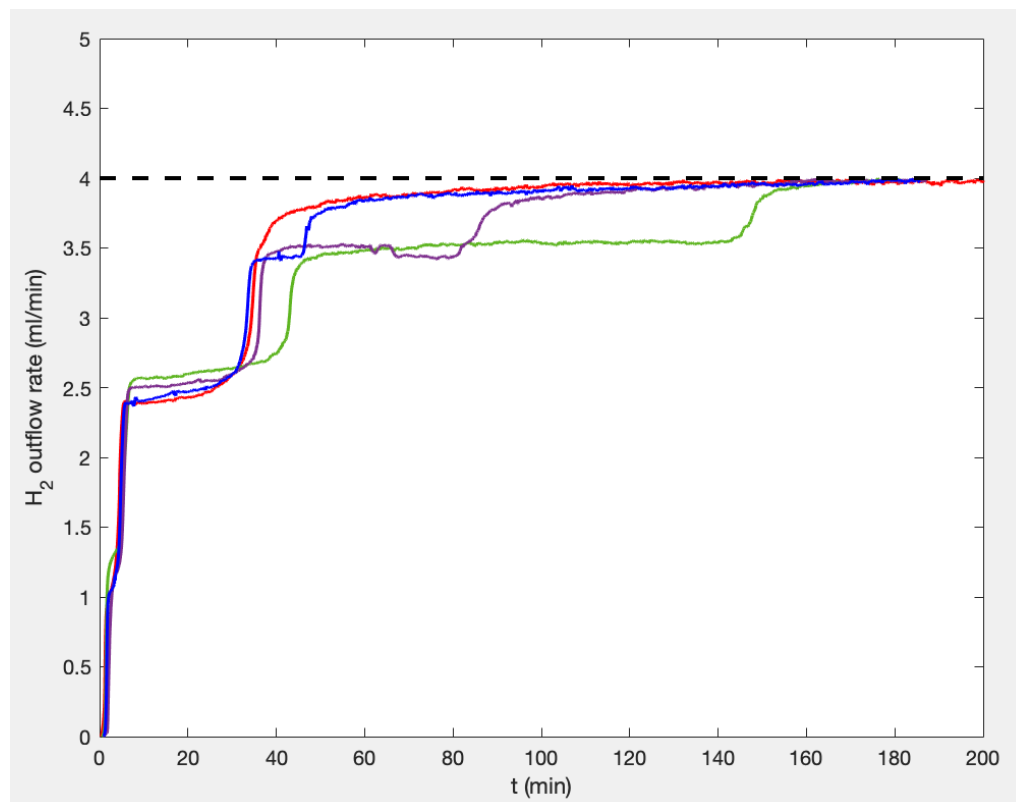


Figure 13 Concentration of hydrogen compared to argon, green (9), purple (10), blue (12), red (14)

5.2.4. Effect of sample size

The final example to be presented, illustrates the role of the sample size in the experiments. As noted in Table 2, most experiments were undertaken with a sample size of (about) 100 mg, but here comparison is made between two reduction experiments (Experiment 12 and 13) under the same conditions, but where double mass was used in the latter (Experiment 13). The outflow rates of H_2 estimated from the MS signals are depicted in Figure 14. As expected, doubling the mass from 100 mg (blue line) to 200 mg (red line) doubles the time taken to reach the different distinct steps, while the levels of the plateaus stay practically unchanged. These tests also illustrate the reproducibility of the results, despite the obvious problems caused by water noted earlier. Finally, it should be noted that the two curves were shifted to start increasing at the same point in time, but in practice the double sample size should also prolong the initial period with no H_2 in the outgoing gas due to a full consumption of the feed H_2 by the hematite-to-magnetite reduction reaction.

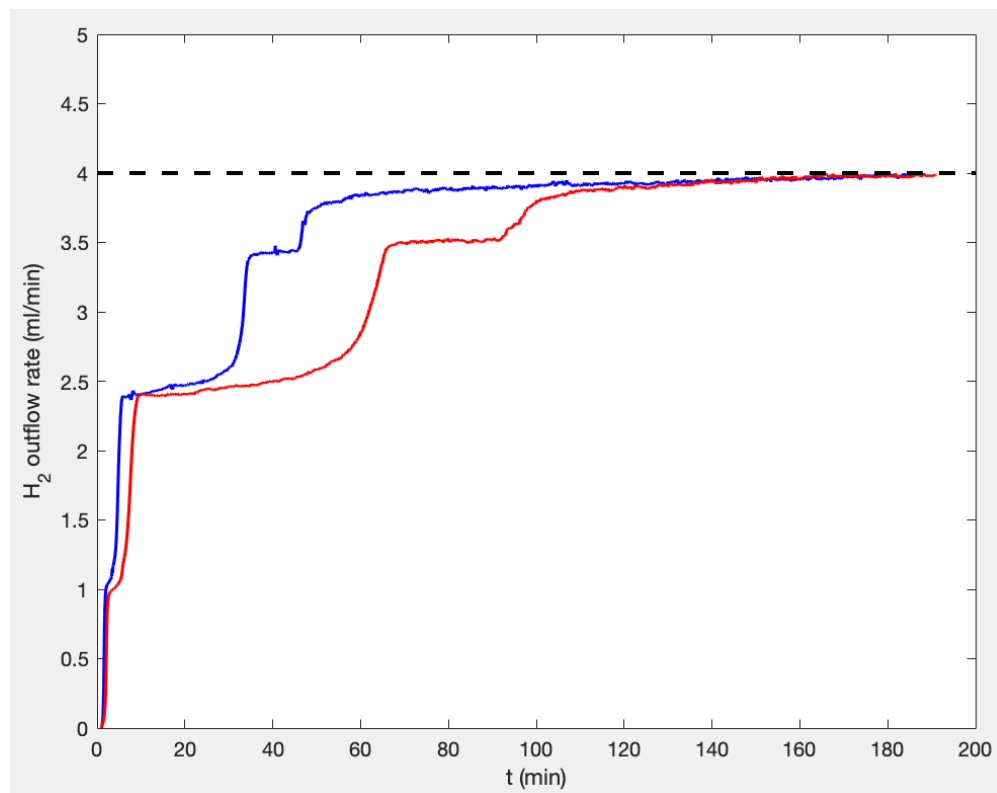


Figure 14 Bed size comparison, blue line (12) red line (13)

5.3. Discussion

Experiments carried out after the primary experiments, further analyzed the signal from the TCD. The obtained data from the TCD and MS signals were plotted in Excel to see the difference between them. The output from the TCD signal can be seen in Figure 15. The temperature in the experiment was 600 °C and the flow rate of H₂ and Ar was 4 ml/min and 8 ml/min respectively.

A possible explanation for the arising problem seen in the end of the reduction curves from the MS throughout the experiments is water affecting the output signal from the MS, as can be seen in Figure 16. The water signal does not mirror the H₂ signal which it should, this in turn indicates that water is causing an error.

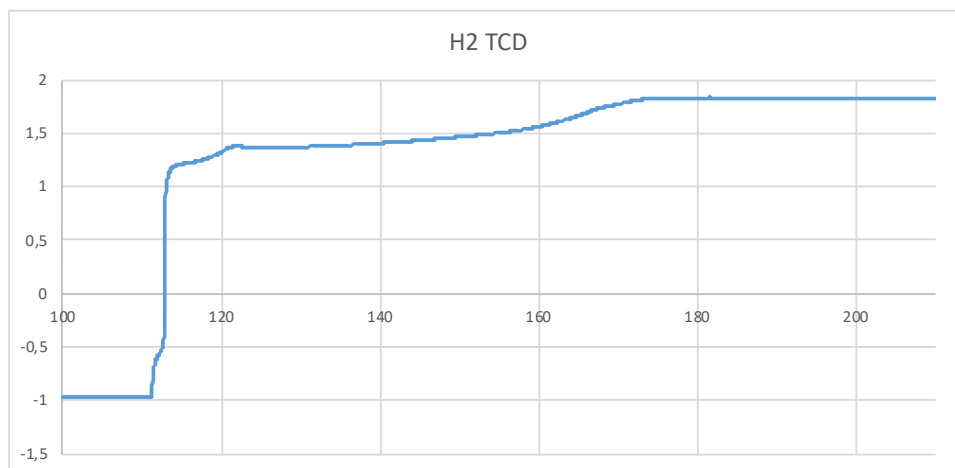


Figure 15 TCD signal

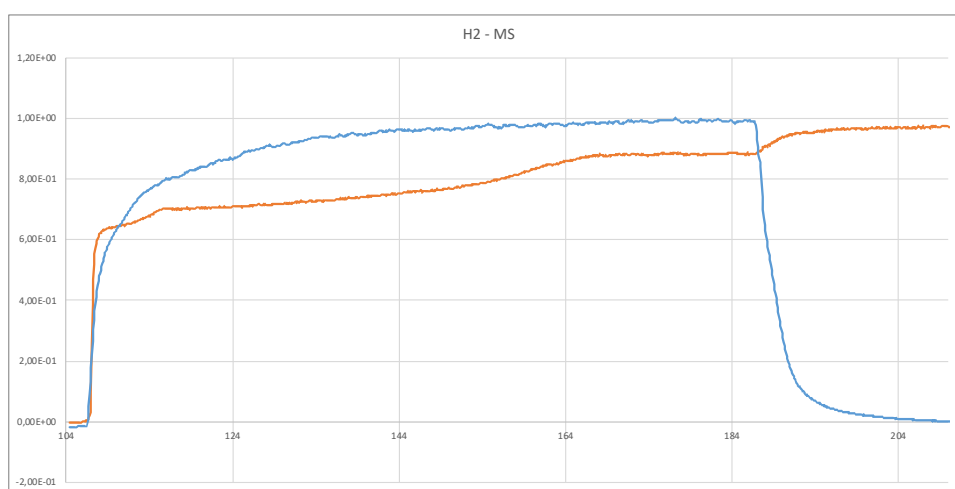


Figure 16 MS signal, blue line H_2O , orange line H_2

The result from the TCD does not show the indescribable plateau seen in previous results from the MS. Comparing Figure 15 and Figure 16 the results from the TCD and MS it can be seen that the first and second plateau is somewhat similar while the last plateau seen from the MS does not occur in the TCD.

This finding indicates that the last tails in the obtained results from the MS should not be included in the calculations. A fast calculation from the TCD signal $(1.8 - 1.35)/(1.8 - -1) = 0.16$ and the MS signal $(1 - 0.72)/1 = 0.28$ suggest an error of $(0.16/0.28 =) 57\%$. This would explain the extraordinarily high reduction degrees obtained from calculations from the MS. This suggest that the signal from the TCD gives a much better indication and the analysis should be based on that.

Finally, some supporting information from mathematically modelling is briefly presented. A three-interface shrinking core model of the reduction reactions of the iron oxides in spherical particles combined by a model of the sample bed developed in the Process and Systems Engineering Laboratory (Salucci, 2022) was used to provide a theoretical view of the experimental conditions. The principles of the model are outlined in the Appendix.

Figure 17 shows the model's predictions of the normalized concentration of H_2 in the gas leaving the sample bed at the bottom, where the normalization was undertaken by dividing the H_2 concentration of the outgoing gas by the corresponding concentration in the feed gas, for different temperatures ranging from 873 K (600 °C) to 1273 K (1000 °C). By comparison of these results with the experimental results reported in Figures 7–14, several similarities can be noted. The plateaus discussed in conjunction with the experiments are clearly noted, and, also how these are shifted with the temperature (Figure 11). Further, a higher temperature is seen to result in more clear plateaus, because of a faster reaction which exhausts the gas of H_2 in the upper part of the sample bed, which makes the conditions approach equilibrium in the lower part of the sample bed.

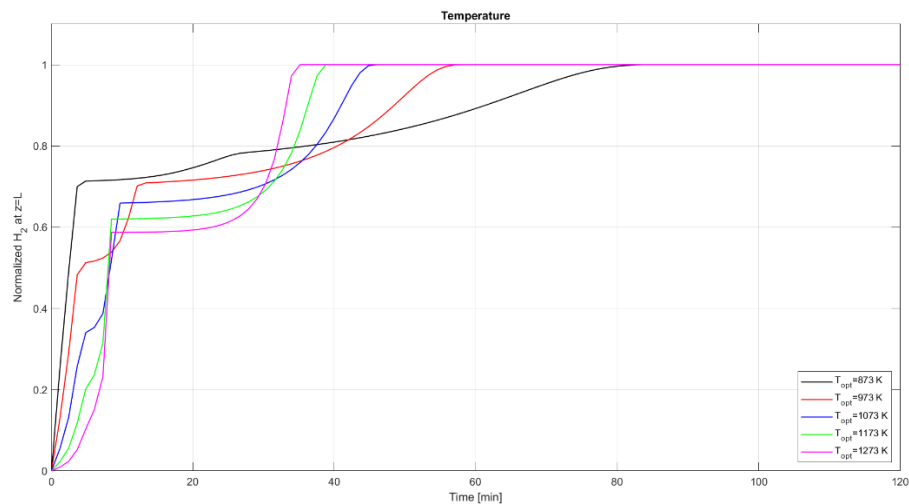


Figure 17 Predictions of the normalized concentration of hydrogen

A more detailed view of the simulated conditions is provided in Figure 18, which shows the simulated conditions in the sample bed for the experiment with the lowest temperature. In the three-dimensional subplots, one of the base axes is the normalized axial position in the sample (0 corresponding to bed top, 1 to bed

bottom) and time (in minutes). The left top panels show the normalized H_2 and H_2O concentrations, while the bottom panels show the reduction degrees (X_i , $i=1,2,3$, see the Appendix) of the three stepwise reduction reactions. These show the expected mirror image of H_2 and H_2O , as well as the fast progress of the first two reduction steps. For the last step, i.e., from wüstite to metallic iron, the conditions in the bed are seen to vary considerably during the first half of the simulation time, where the particles in the upper part of the bed get fully reduced much earlier than the particles in the lower part. After about 80 minutes, the whole bed is fully reduced, as seen in the top right panel, which depicts the normalized H_2 concentration of the gas that leaves the bed.

It should be noted that the kinetic parameters and diffusion coefficients in the particle and the bed were set partly based on results reported in the literature and partly by trial-and-error, and that the goal was not to reproduce a particular experiment but merely to show a theoretical interpretation of the experimental findings.

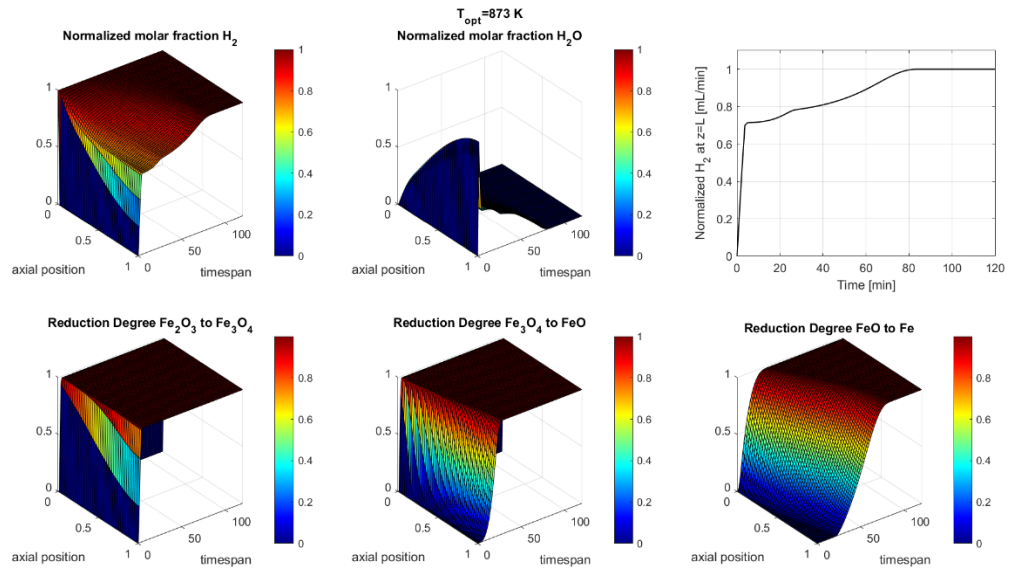


Figure 18 Simulated conditions in the sample bed for the experiment with the lowest temperature

5.4. Conclusions and further studies

A number of reduction experiments of iron oxides in hydrogen-containing gas in small scale have been undertaken and presented in this thesis. The results from the experiments were largely supported by findings reported in the literature and preliminary simulations. (Salucci, 2022) However, several problems in using the MS signal to reconstruct the concentrations in the outgoing gas were noted, which made it impossible to reliably estimate the overall reduction degree of the samples.

It can be concluded that the reduction time with H₂ was highly dependent on temperature. Despite the small particle (< 5 μm) and sample (100–200 mg) sizes, the reduction took over 200 minutes at 400 °C and did not in all cases reach completion. At higher temperatures, e.g., 600 °C, the time to reach complete reduction was about 75 minutes, and at 800 °C about 50 minutes. More detailed analysis of the effect of H₂ concentration should however be undertaken after solving the measurement problems discussed below.

Even though the results have shed some light on the reduction of iron oxides by H₂, it is obvious that more experiments should be carried out to get a more extensive data set for the modeling of the process. Also, some of the experiments could be done again to verify that the results are reproducible.

Another obvious way of improving the quality of the information obtained in the experiments is to analyze the reduced samples with respect to the final composition and structure, e.g., by XRD and SEM. This could verify that the samples reduced at high temperature have reached full conversion and estimate how much oxides (wüstite) is left in experiments undertaken at low temperature or experiments interrupted at an earlier stage. It could also provide information about the structure of the particles (reacted layers, porosity, etc.). A problem noted was that the samples were highly reactive so metallic iron rapidly oxidized if it was exposed to air even after being cooled to low temperatures. Therefore, to prevent re-oxidation the samples must be quenched and stored in an inert gas before being analyzed.

The abnormalities in the end of the reduction curve could be further studied to verify the reason for the problem. The brief study presented in section 5.3 indicates that it would presumably be better to base the analysis on the TCD signal instead of the MS signal, since the former is more quantitative and should not be disturbed by the presence of water. Using the present MS signal, it was not possible to close the balances in a reasonable way, so the overall reduction degree could not be determined at any reasonable accuracy.

6. SUMMARY IN SWEDISH – SVENSK SAMMANFATTNING

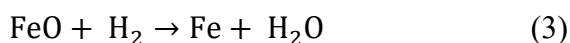
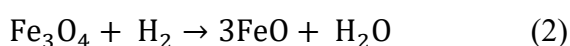
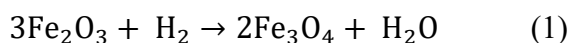
Experimentell studie av reduktion av järnmalm med vätgas

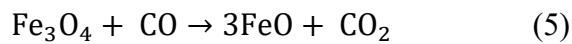
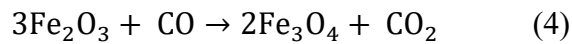
De ökade utsläppen av koldioxid, CO₂, är en stor bidragande orsak till den klimatförändring som nu kan observeras. Stål- och järnindustrin står för 7–9% av de totala koldioxidutsläppen. (Spreitzer & Schenk, 2019) Stål- och järnindustrin har en stor ekonomisk betydelse i världen samt en stor betydelse för levnadsstandarden. Runtom i världen producerades 1,8 miljarder ton råstål år 2020. Genom återvinning av stål minskar utsläppen, dock inte tillräckligt. Att helt lägga ner tillverkningen av stål är inte möjligt, men däremot är det en nödvändighet att undersöka och hitta mer miljövänliga sätt att tillverka stål för att den globala uppvärmningen inte ska överskrida klimatmålet på 2 °C. (Ghosh & Chatterjee, 2008)

Under de senaste åren har alternativa sätt att framställa järn utretts. Ett av dessa är att i stället för kolmonoxid, CO, använda vätgas, H₂, vid reducering av järnoxider. Vätgas har högt värmevärde, hög värmeledningsförmåga och hög reaktionshastighet. Dessa egenskaper gör att gasen har stor potential inom järnindustrin. (Liu, et al., 2020)

Utvecklingen går ständigt framåt och i detta diplomarbete har experiment med vätgas som reduktionsmedel utförts och analyserats vid Åbo Akademis laboratorium. Resultaten har jämförts med tidigare teorier och tidigare utförda experiment inom ämnet. Experimenten har gjorts vid olika temperaturer, massflöden och storlek på reaktionsbädden. Genom att utföra experimenten har data samlats in för att få fram kinetiska parametrar för att kunna modellera vätgasreduktionen för att slutligen kunna simulera reduktionen.

Vid användning av kolmonoxid och vätgas som reduktionsmedel sker reaktionerna med järnoxiden enligt följande heterogena reaktioner:





Beroende på den reducerande gasen, vätgas eller kolmonoxid, bildas antingen vatten, H₂O, eller koldioxid när järnoxiderna reagerar. När hematit, Fe₂O₃, reagerar med den reducerande gasen resulterar det i magnetit, Fe₃O₄, och antingen H₂O (1) eller CO₂ (4). Ytterligare reaktion med magnetit resulterar i wüstit, FeO, och H₂O (2) eller CO₂ (5). Slutligen resulterar reaktion med wüstit i järn, Fe, och H₂O (3) eller CO₂ (6).

Med vätgas och vid temperaturer över 843 K går reduktionen från hematit via magnetit till wüstit och slutligen till järn. Temperaturer under 843 K resulterar i en reduktion direkt från magnetit till metalliskt järn. Detta kan ses i Baur-Glässner-diagrammet, Figure 3. (Spreitzer & Schenk, 2019)

För att uppnå högsta utnyttjande av den reducerande gasen förväntas avslutningen av reduktionen ske vid en specificerad temperatur i jämviktstillståndet. Reduktionsanalysen är alltså baserad på jämviktsdiagrammet se Figure 3. (Chen, et al., 2019)

I Figure 3 visas Baur-Glässner-diagrammet för Fe-O-H₂-systemet i förhållande till temperatur och gasoxidationsgrad (GOD). Stabilitetsområdena för olika järnoxidfaser visas beroende på temperatur och GOD. Definitionen för GOD är förhållandet mellan de oxiderade gaskomponenterna samt summan av de oxiderade och oxiderbara föreningarna. (Spreitzer & Schenk, 2019)

I diagrammet kan ses att högre temperaturer resulterar i ett större stabilitetsområde för metalliskt järn och wüstit. En lägre GOD karakteriserar en högre reduktionskraft för gasblandningen. Detta indikerar att ur termodynamisk synvinkel bör reduktionen med vätgas utföras vid högsta möjliga temperatur. (Spreitzer & Schenk, 2019) Vid lägre temperaturer är stabilitetsytan för järn mindre och därmed kan en mindre mängd järn erhållas.

Högre temperatur ökar reduktionshastigheten och är också fördelaktigt i termer av kinetik, tack vare de begränsande effekterna avseende diffusion och kärnbildning. Dessutom minskar den kemiska reaktionen. Arrhenius ekvation är ett matematiskt uttryck som beskriver temperaturens effekt på kemiska reaktioners hastighet. Enligt Arrhenius ekvation kommer en stigande temperatur att leda till en reduktionshastighet som ökar exponentiellt. (Spreitzer & Schenk, 2019)

$$k = Ae^{-\frac{E_a}{RT}} \quad (10)$$

I ekvationen är k reaktionshastighetskonstanten, A frekvensen vid vilken molekylerna och atomerna kolliderar, $R = 8,314 \text{ J}/(\text{mol}\cdot\text{K})$ den ideala gaskonstanten, E_a aktiveringsenergin och T den termodynamiska temperaturen. (Gregersen, 2019)

Huvuduppsättningen för experimenten var densamma i alla experiment. Experimenten utfördes isotermiskt vid atmosfärstryck. För att kunna utvärdera reduktionen av hematit och magnetit med vätgas har olika reduktionsexperiment gjorts. Experimenten har utförts vid olika temperaturer och med olika massflöden. Vissa experiment har även gjorts utan prov för att få en baslinje för analysen, se tabell 2. I experimenten har argon använts som inert gas.

Initialt placerades kvartsull i reaktionsröret. Järnoxidpulver uppmättes till önskad mängd och placerades på kvartsullen i röret. När proverna placerats i röret och röret satts på plats angavs förutsättningarna för experimenten i utrustningens datorprogram. För att nå den önskade temperaturen vid varje experiment ökades temperaturen $10 \text{ }^\circ\text{C}/\text{min}$ tills önskad temperatur uppnått. När temperaturen hölls stabil under hela experimentet. Argon och vätgas lagrades i komprimerade gasflaskor och gasernas massflöden styrdes av de villkor som ställdes i datorprogrammet. I början av varje experiment släpptes argon igenom systemet tills önskad temperatur uppnått. När önskad temperatur uppnått öppnades vätgasventilen manuellt. Experimenten varade tills reduktionen var komplett varpå nedkyllning påbörjades. Argonatmosfär bibehölls under både uppvärmning och nedkyllning.

Experimenten utfördes, som framgår av tabell 2, vid temperaturer från 400 °C till 900 °C. Massflödet av vätgas varierade från 2 ml/min till 20 ml/min och massflödet av argon varierade från 0 ml/min till 24 ml/min.

Resultatet från experimenten överensstämmer med den teori som finns och tidigare experiment som utförts. De data som samlats in från experimenten har även kunnat användas för simulering av reduktion av järnmalm med vätgas vilket var målet med arbetet, men först måste mätproblemen som förmodligen förorsakades av alltför hög vattenhalt in gasen som sänds till masspektrometern lösas. Ett gångbart alternativ är att i stället använda den befintliga värmeledningsmätningen som utgångspunkt.

7. REFERENCES

- Bonalde, A., Henriquez, A. & Manrique, M., 2005. *Kinetic Analysis of the Iron Oxide Reduction Using Hydrogen-Carbon Monoxide Mixtures as Reducing Agent.*, u.o.: ISIJ International.
- Cavaliere, P., 2019. *Direct Reduced Iron: Most Efficient Technologies for Greenhouse Emissions Abatement.* [Online] Available at: https://link.springer.com/chapter/10.1007/978-3-030-21209-4_8#citeas [Använd 24 January 2022].
- Chen, Z. o.a., 2019. *Review and data evaluation for high-temperature reduction of iron oxide particles in suspension*, u.o.: Taylor & Francis Online.
- El-Geassy, A. & Nasr, M. I., 1988. *Influence of the Original Structure on the Kinetics of Hydrogen Reduction of Hematite Compacts*, Cairo: Central Metallurgical Research and Development.
- El-Gleassy, A. A., El- Kashif, F. O., Nasr, M. I. & Omar, A. A., 1994. *Kinetics and Mechanisms of Re-oxidation of Freshly Reduced Iron Compacts*, Helwan: Central Metallurgical Research and Development Institute.
- Elzohiery, M., Sohn, H. Y. & Muhassab, Y., 2016. *Kinetics of Hydrogen Reduction of Magnetite Concentrate Particles in Solid State Relevant to Flash Ironmaking*, Weinheim: Steel research.
- Fruehan, R. J., Brabie, L. & Kim, E.-J., 2005. *Final stage of reduction of iron ores by hydrogen*, Pittsburgh: Scandinavian Journal of Metallurgy.
- Ghadi, A. Z., Valipour, M. S., Vahedi, S. M. & Sohn, H. Y., 2020. *A Review on the Modeling of Gaseous Reduction of Iron Oxide Pellets*, u.o.: Steel Research int..
- Ghosh, A. & Chatterjee, A., 2008. *Ironmaking and Steelmaking theory and practice*, New Delhi: PHI Learning.
- Gregersen, E., 2019. *Arrhenius equation.* [Online] Available at: <https://www.britannica.com/science/Arrhenius-equation> [Använd 25 Mars 2022].
- Gregersen, E., 2022. *Blast Furnace.* [Online] Available at: <https://www.britannica.com/technology/blast-furnace> [Använd 12 april 2022].
- Habermann, A. o.a., 2000. *An Experimental Study on the Kinetics of Fluidized Bed Iron Ore Reduction*, Vienna: ISIJ International.

- Hara, Y., Sakawa, M. & Kondo, S., 1976. *Tetsu to Hagane*, u.o.: u.n.
- Hoffman, C., Van Hoey, M. & Zeumer, B., 2020. *Decarbonization challenge for steel*, u.o.: McKinsey & Company.
- Kazemi, M., 2016. *Fundamental Studies Related to Gaseous Reduction of Iron Oxide*, Stockholm: KTH Royal Institute of Technology.
- Liu, W. o.a., 2020. *The production and application of hydrogen in steel industry*, Beijing: ScienceDirect.
- Pineau, A., Kanari, N. & Gaballah, I., 2005. *Kinetics of reduction of iron oxides by H₂: Part I: Low temperature reduction of hematite*, Vandœuvre: ScienceDirect.
- Pourhakkak, P. o.a., 2021. *Fundamentals of adsorption technology*. [Online] Available at: <https://www.sciencedirect.com/science/article/pii/B9780128188057000011> [Använd 18 April 2022].
- Salucci, E., 2022. *Unpublished manuscript*, Åbo: Åbo Akademi University.
- Shao, L. o.a., 2021. *A numerical study on the operation of the H₂ shaft furnace with top gas recycling*, u.o.: Metallurgical and Materials Transactions.
- Spreitzer, D. & Schenk, J., 2019. *Iron Ore Reduction by Hydrogen Using a Laboratory Scale Fluidized Bed Reactor: Kinetic Investigation—Experimental Setup and Method for Determination*, 2471–2484: Metall Mater Trans B.
- Spreitzer, D. & Schenk, J., 2019. *Reduction of Iron Oxides with Hydrogen—A Review*. [Online] Available at: <https://onlinelibrary.wiley.com/doi/full/10.1002/srin.201900108> [Använd January 2022].
- Walker, R. D., 2017. *Iron processing*. [Online] Available at: <https://www.britannica.com/technology/iron-processing> [Använd 24 January 2022].
- Wei, Z. o.a., 2018. *Reduction kinetics of hematite ore fines with H₂ in a rotary drum reactor*, Taiyuan: ScienceDirect.
- Weiss, B., 2010. Structural and morphological changes during reduction of hematite to magnetite and wustite in hydrogen rich reduction gases under fluidised bed conditions. *Ironmaking & Steelmaking*, January.
- Yang, Y., Raipala, K. & Holappa, L., 2013. *sciencedirect.com*. [Online] Available at:

<https://www.sciencedirect.com/science/article/pii/B9780080969886000171>

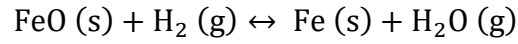
[Använd 25 Mars 2022].

Zuo, H.-b.o.a., 2015. *Reduction kinetics of iron oxide pellets with H₂ and CO mixtures*, u.o.: International Journal of Minerals, Metallurgy, and Materials.

APPENDIX 1

This appendix briefly outlines the theory behind an unreacted three-interface shrinking core model developed by (Salucci, 2022) on the basis of the original work of (Hara, et al., 1976) further developed in (Shao, et al., 2021) and its application to describe the small particle bed in the experimental setup of the thesis.

The basic concepts of the model is explained below using a simplified case, i.e., a one-interface shrinking core model for the wüstite reduction to metallic iron by hydrogen.



In this model, the reduction degree, X , can be expressed as:

$$X(t) = \frac{m_0 - m(t)}{m_0} = \frac{\frac{4}{3}\pi\rho(r_0^3 - (r(t))^3)}{\frac{4}{3}\pi\rho r_0^3} = 1 - \left(\frac{r(t)}{r_0}\right)^3 \quad (\text{A1})$$

where m , r and ρ are the mass, radius and density of the particle and subscript 0 refers to the initial state. In the equation, $r(t)$ is the time-dependent radius of the interface of the unreacted core. The relationship describes the dependence between the reduction degree and the radius of the unreacted core, which considerably simplifies the calculation.

Further assumptions applied are that the

- total gas concentration is constant
- the reacted layer has a radially homogeneous porosity
- the temperature and pressure of the gas inside the particle are constant
- the changes in the internal gas profiles are fast and can be assumed to be in a steady-state

Based on these assumptions, and after some algebra, the overall reduction rate can be expressed as:

$$N(t) = \frac{c_{\text{H}_2,\text{bulk}}}{\frac{1}{k_c} \frac{1}{(1-X(t))^{2/3}} + \frac{r_0}{D_{\text{eff}}} \left(\frac{1}{K} + 1\right) \frac{1-(1-X(t))^{1/3}}{(1-X(t))^{1/3}} + \left(\frac{1}{Kh_{\text{H}_2\text{O}}} + \frac{1}{h_{\text{H}_2}}\right)} \quad (\text{A2})$$

The first, second and third terms in the denominator are the resistances caused by chemical kinetics, internal and external diffusion. In the equation, $c_{\text{H}_2,\text{bulk}}$ is the hydrogen concentration in the bulk gas, k_c is the reaction rate constant, D_{eff}

represents the effective diffusion coefficient in the particle, K is the equilibrium constant of the chemical reaction and h represents the external mass transfer coefficient of the gaseous species, i.e., of the boundary layer around the particle. Typically, the chemical reaction represents the limiting step at low temperatures (kinetic regime). As the temperature increases, the reaction rate increases more rapidly (cf. exponential dependence of the kinetic constant, Arrhenius law) than the diffusion phenomena (dependence on power laws). Therefore, theoretically, as the temperature increases, the reaction rate will become diffusion limited.

By extending the present model to study to all the reactions involved in the process, the model becomes a three-interface shrinking core model, as schematically depicted in Figure A1. This model is an extension of the two interface SCM presented in Melchiori (2014) with reversible reactions describing the reduction of a single pellet. In the model, the conversion degrees of the three oxides in the reactions, $X_j, j = 1, \dots, 3$, can be related to the ratio of the three interfaces in a similar way as done in Eq. (A1). The reader is referred to (Shao, et al., 2021) for a brief description of the model.

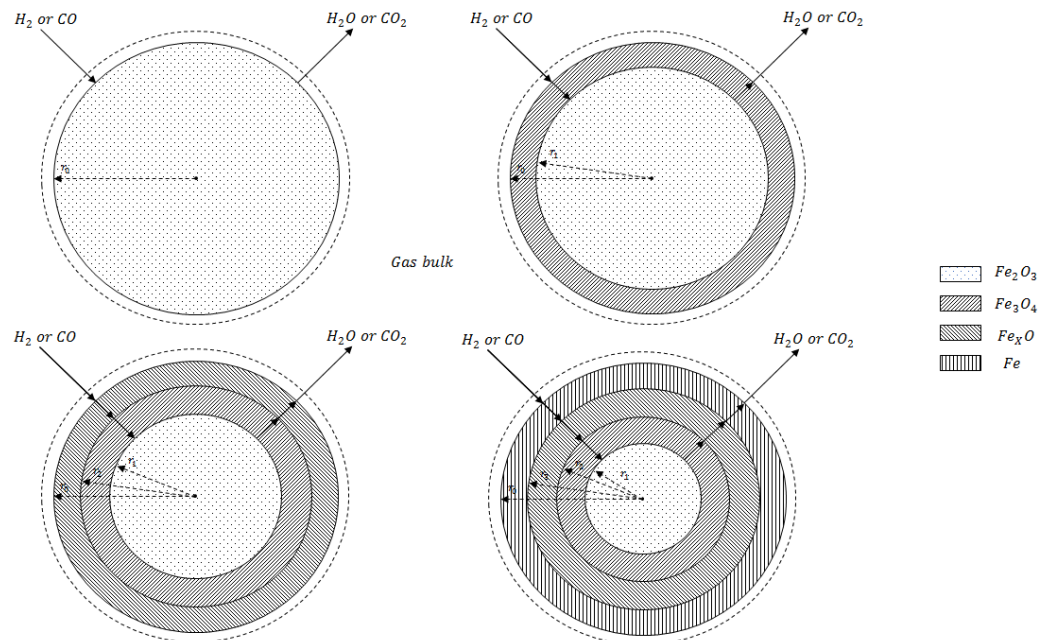


Figure A1 Three-interface shrinking core model on the reduction of a hematite particle

Further, since the reactions in the experimental setup occur in a bed of particles, i.e., the sample in the experiments, the local gas and solid compositions must be considered, since the hydrogen and water content of the gas change as the gas passes through the bed. The thermal conditions are here simplified by assuming that the temperature is constant, i.e., that isothermal conditions prevail. Thus, in addition to the dependence on time, a dependence on the (normalized) vertical position in the bed, z , has to be considered. The mass balance equations in differential form for this system are:

$$\frac{\partial X_j(t,z)}{\partial t} = \frac{N(t,z)}{n_0 a_j} \quad (\text{A3})$$

$$\frac{\partial c_{\text{H}_2}(t,z)}{\partial t} = -\frac{u_g}{h} \frac{\partial c_{\text{H}_2}(t,z)}{\partial z} + \frac{D_b}{h^2} \frac{\partial^2 c_{\text{H}_2}(t,z)}{\partial z^2} - \frac{1}{1-\varepsilon_b} \sum_{j=1}^3 N_j(t,z) \quad (\text{A4})$$

$$\frac{\partial c_{\text{H}_2\text{O}}(t,z)}{\partial t} = -\frac{u_g}{h} \frac{\partial c_{\text{H}_2\text{O}}(t,z)}{\partial z} + \frac{D_b}{h^2} \frac{\partial^2 c_{\text{H}_2\text{O}}(t,z)}{\partial z^2} + \frac{1}{1-\varepsilon_b} \sum_{j=1}^3 N_j(t,z) \quad (\text{A5})$$

where j ($=1,2,3$) is the number of the reaction in the step-wise conversion of hematite to metallic iron by hydrogen. The first, second and third terms on the right-hand-sides of Eqs. (A4-A5) are the convection, dispersion and consumption/production terms in the bed. In the equations, n_0 is the initial oxygen content in the solid phase, a_j represents a parameter for the initial oxygen content which depends on the type of iron oxide to be reduced, u_g is the velocity of the gas entering the bed, D_b is the axial dispersion coefficient while ε is the voidage of the bed.

Finally, boundary conditions of the system of partial differential equations must be given for the bed inlet ($z = 0$) and outlet ($z = 1$)

$$c_{\text{H}_2}(t, 0) = c_{\text{H}_2,\text{bulk}} ; \quad c_{\text{H}_2\text{O}}(t, 0) = 0 \quad (\text{A6, A7})$$

$$\left. \frac{\partial c_{\text{H}_2}(t,z)}{\partial z} \right|_{z=1} = 0 ; \quad \left. \frac{\partial c_{\text{H}_2\text{O}}(t,z)}{\partial z} \right|_{z=1} = 0 \quad (\text{A8, A9})$$

The model requires pertinent values of thermochemical properties of the gaseous components, thermodynamic data, mass transfer coefficient and chemical reaction rates, as well as a procedure for the solution of the equations. In the numerical examples presented in the thesis, the method of lines was applied to solve the partial differential equations. (Salucci, 2022)

APPENDIX 2

SIGMA-ALDRICH®

sigma-aldrich.com

3050 Spruce Street, Saint Louis, MO 63103, USA

Website: www.sigmaaldrich.com

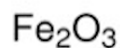
Email USA: techserv@sial.com

Outside USA: eurtechserv@sial.com

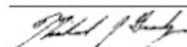
Certificate of Analysis

Product Name:
Iron(III) oxide - powder, <5 µm, ≥96%

Product Number: 310050
Batch Number: MKCL9079
Brand: SIGALD
CAS Number: 1309-37-1
MDL Number: MFCD00011008
Formula: Fe₂O₃
Formula Weight: 159.69 g/mol
Quality Release Date: 12 FEB 2020



Test	Specification	Result
Appearance (Color)	Red to Very Dark Red and Brown-Red and Brown-Red Brown-Orange	
Appearance (Form)	Powder	Powder
Titration with Na ₂ S ₂ O ₃ % Iron	96.0 - 104.0 %	96.1 %
ICP Major Analysis Confirms Iron Component	Confirmed	Confirmed
Size Particle Size Measurements	< 5 micron	1 micron



Michael Grady, Manager
Quality Control
Milwaukee, WI US

Sigma-Aldrich warrants, that at the time of the quality release or subsequent retest date this product conformed to the information contained in this publication. The current Specification sheet may be available at Sigma-Aldrich.com. For further inquiries, please contact Technical Service. Purchaser must determine the suitability of the product for its particular use. See reverse side of invoice or packing slip for additional terms and conditions of sale.

Version Number: 1

Page 1 of 1

APPENDIX 3

SIGMA-ALDRICH

sigma-aldrich.com

3050 Spruce Street, Saint Louis, MO 63103, USA

Website: www.sigmaaldrich.com

Email USA: techserv@sial.com

Outside USA: eurtechserv@sial.com

Product Specification

Product Name:
Iron(II,III) oxide - powder, <5 µm, 95%

Product Number: 310069
CAS Number: 1317-61-9
MDL: MFCD00011010
Formula: Fe₃O₄
Formula Weight: 231.53 g/mol



TEST	Specification
Appearance (Color)	Black
Appearance (Form)	Powder
X-Ray Diffraction	Conforms to Structure
Titration with Na ₂ S ₂ O ₃ % Fe	68.0 - 76.7 %
Size (Average Particle Size)	≤ 5 micron

Specification: PRD.0.ZQ5.10000058676

Sigma-Aldrich warrants, that at the time of the quality release or subsequent retest date this product conformed to the information contained in this publication. The current Specification sheet may be available at Sigma-Aldrich.com. For further inquiries, please contact Technical Service. Purchaser must determine the suitability of the product for its particular use. See reverse side of Invoice or packing slip for additional terms and conditions of sale.

1 of 1